Supplementary Materials

A Geometrical Berry Phase Induced in Im-3m H3S at 200GPa by Ultra-fast Laser Pulses

1. Supplementary Materials S1. NG-QTAIM theoretical background and procedure to generate the Hessian of $\rho(\mathbf{r})$ eigenvector-following trajectories $\mathsf{T}(s)$.

2. Supplementary Materials S2. Hessian of $\rho(\mathbf{r})$ partitioning scheme scalar QTAIM measures for the 200 GPa *Im-3m*-H_3S crystal graph.

3. Supplementary Materials S3. Variation of the 200 GPa *Im-3m*-H_3S crystal graph ellipticity ε with time and the carrier-envelope phase (CEP) angle ϕ.

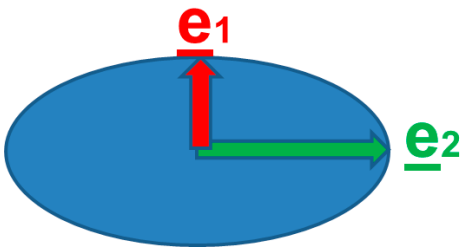
4. Supplementary Materials S4. Tables and trajectories $\mathsf{T}(s)$ of the 200 GPa *Im-3m*-H_3S crystal graph.

5. Supplementary Materials S5. Tables and trajectories $\mathsf{T}(s)$ of the 200 GPa *Im-3m*-H_3S crystal graph S7---S8 *BCP*.

1. Supplementary Materials S1. NG-QTAIM theoretical background and procedure to generate the Hessian of $\rho(\mathbf{r})$ eigenvector-following trajectories $\mathsf{T}(s)$.

1(a) *QTAIM bond critical point (BCP) properties; ellipticity ε:*

The four types of QTAIM critical points are labeled using the notation (R, ω) where R is the rank of the Hessian matrix, i.e., the number of distinct non-zero eigenvalues and ω is the signature (the algebraic sum of the signs of the eigenvalues); the (3, -3) [nuclear critical point (*NCP*), a local maximum], (3, -1) and (3, 1) [saddle points, referred to as bond critical points (*BCP*) and ring critical points (*RCP*), respectively] and (3, 3) [the cage critical points (*CCP*)]. In the limit that the forces on the nuclei are zero, an atomic interaction line the line passing through a *BCP* and terminating on two nuclear attractors along which the charge density $\rho(\mathbf{r})$ is locally maximal with respect to nearby lines, becomes a bond-path. The full set of critical points with the bond-paths of a molecule or cluster is referred to as the molecular graph.



Scheme S1. The cross section through a bond at the bond critical point (*BCP*). The λ_1 and λ_2 eigenvalues with associated eigenvectors $\underline{\mathbf{e}}_1$ and $\underline{\mathbf{e}}_2$ respectively, define the axes of the ellipse and indicate the magnitudes of the least and greatest extents of the distribution of $\rho(\mathbf{r})$.

The ellipticity, ε, defined as $\varepsilon = |\lambda_1|/|\lambda_2| - 1$, quantifies the relative accumulation of the electronic charge density $\rho(\mathbf{r_b})$ distribution in the two directions $\underline{\mathbf{e}}_1$ and $\underline{\mathbf{e}}_2$ that are perpendicular to the bond-path at a Bond Critical Point (*BCP*) with position $\mathbf{r_b}$. For ellipticity $\varepsilon > 0$, the shortest and longest axes of the elliptical distribution of $\rho(\mathbf{r_b})$ are associated with the λ_1 and λ_2 eigenvalues, respectively. From the electron-preceding perspective a change in the electronic charge density distribution that defines a chemical bond causes in a change in atomic positions. Bone and Bader later proposed that the direction of motion of the atoms that results from a slightly perturbed structure coincides with the direction of motion of the electrons; this was later confirmed.

1(b) *The eigenvector-space trajectories*: $\mathsf{T}_i(s)$; $i = \{\rho\}$ *for Stereochemistry:*

The maximum eigenvector projections $\mathsf{T}(s)_{\mathbf{max}} = \{t_{1\mathbf{max}}, t_{2\mathbf{max}}, t_{3\mathbf{max}}\}$ are used to define the dimensions of a 'bounding box' around each $\mathsf{T}(s)$ and are used to calculate the chirality C, bond-flexing F and bond-axiality A. The subscript '$_{\mathbf{max}}$' corresponds to the difference between the minimum and maximum value of the projection of the

BCP shift **dr** onto $\underline{\mathbf{e}}_1$, $\underline{\mathbf{e}}_2$ or $\underline{\mathbf{e}}_3$ along the entire $\mathsf{T}(s)$. Note: the $\mathbf{e}_2$ corresponds to the direction in which the electrons at the *BCP* are subject to the most compressive forces, therefore $\mathbf{e}_2$ corresponds to the most *facile direction* for displacement of the *BCP* electrons when the *BCP* is torsioned. Conversely the $\mathbf{e}_1$ and $\mathbf{e}_3$ correspond to the directions associated with the least compressive forces and the tensile forces on the *BCP* electrons respectively.

1(c) *Numerical Considerations for Calculation of the Eigenvector-Space Trajectory $\mathsf{T}_i(s)$*

Central to the concept of the second-generation eigenvector-space trajectory $\mathsf{T}_i(s)$ is the concept of a monotonically increasing sequence parameter s, which may take the form of an increasing integer sequence (0, 1, 2, 3,...) in applications where a set of discrete numbered steps are involved, or a continuous real number. The 3-D eigenvector trajectory $\mathsf{T}_i(s)$ is then defined as an ordered set of points, whose sequence is described by the parameter s. In this application, we used an integer step number for s. We first choose to associate $s = 0$ with a specific reference molecular graph, in this case, the energy minimum structure. For a specific *BCP*, the coordinates associated with each of the points are calculated by evaluating the components of the shift vector $\mathbf{dr} = \mathbf{r_b}(s) - \mathbf{r_b}(s\text{-}1)$ where $\mathbf{r_b}$ indicates the location of the *BCP*, from the previous step to the current step in the reference coordinate frame defined by the eigenvectors $\underline{\mathbf{e}}_1$, $\underline{\mathbf{e}}_2$, $\underline{\mathbf{e}}_3$.

Note: for <u>displaying</u> the eigenvector trajectories $\mathsf{T}_i(s)$, large steps that can occur at the beginning or end of a $\mathsf{T}_i(s)$ may swamp the appearance of the $\mathsf{T}_i(s)$. To solve this we temporarily filter these steps before including them back in to correctly calculate the U_σ-space eigenvector trajectory $\mathsf{T}_i(s)$.

The calculation of the $\mathsf{T}_i(s)$ is made easier if the code which produces the list of structures corresponding to points along each step of the torsion (CW) and counterclockwise CCW generates these structures at regularly-spaced points. The consequence of this desirable characteristic is that there are few or no large changes or 'spikes' in the magnitude of the *BCP* shift vector **dr** i.e. $\Delta\mathbf{dr}$, between path step $\boldsymbol{s}$ and $\boldsymbol{s} + 1$. Such anomalies occur because some path-following algorithms may employ occasional small predictor-corrector steps that are at least an order of magnitude smaller than standard steps. In this analysis it is observed that such intermittent relatively small steps in turn cause very small shifts **dr** to be interspersed between longer runs of larger changes, causing 'spike' noise in the otherwise smooth trajectories $\mathsf{T}_i(s)$. Such 'spikes', which usually only consist of a single spurious point deviating from the locally smooth eigenvector trajectory, can make potentially large spurious contributions to the eigenvector trajectory $\mathsf{T}_i(s)$ and may be safely filtered. A combination of criteria are recommended for automated rejection of inclusion of a specific point into the trajectories $\mathsf{T}_i(s)$:

1. If the magnitude of the **dr** associated with any current $\mathsf{T}_i(s)$ point is less than 50% of the average of the corresponding **dr** values associated with the immediately preceding point and the immediately following point,

the current point is filtered out as a ‘spike’.

2. Abrupt changes in direction in the $\mathsf{T}_i(s)$, e.g. turning by more than 60^0 from one $\mathsf{T}_i(s)$ step to the next cause the current point to be labelled as a ‘spike’.

These two rules taken together are referred to as the ‘turn’ filter. These rules can be repeatedly applied across multiple ‘passes’ through the eigenvector trajectory data as necessa ry.

It has been observed that the magnitudes of the steps **dr** naturally tend to slowly decrease toward the end of paths, corresponding to a slowed approach to an end minimum, and the corresponding part of the $\mathsf{T}_i(s)$ turns toward the U_i-space origin. A combination of the criteria mentioned above may be deployed to retain these parts of the $\mathsf{T}_i(s)$.

2. Supplementary Materials S2. Hessian of $\rho(\mathbf{r})$ partitioning scheme scalar QTAIM measures for the 200 GPa *Im-3m*-H_3S crystal graph.

Table S2(aI). The fractional coordinates for the S7-H3 *BCP*s of the Hessian of $\rho(\mathbf{r})$ partitioning scheme measures for the 200 GPa *Im-3m*-H_3S crystal graph in the absence of an applied E-field and also with variation in the carrier-envelope phase

(CEP) angle ϕ corresponding to the 5 femtosecond peaks of the **CW (R, [+1])** and **CCW (S, [-1])** pulses, see **Scheme 1** of the main text and **Table S2(a)**.

fractional coordinates

zero E-field
(0.5000, 0.5000, 0.1653)

ϕ	**CW (R, [+1])**	**CCW (S, [-1])**
0°	(0.5000, 0.5003, 0.1606)	(0.5000, 0.5003, 0.1599)
30°	(0.5000, 0.5000, 0.1617)	(0.5000, 0.5000, 0.1589)
60°	(0.5000, 0.4997, 0.1624)	(0.5000, 0.4997, 0.1583)
90°	(0.5000, 0.4995, 0.1625)	(0.5000, 0.4996, 0.1581)
120°	(0.5000, 0.4993, 0.1620)	(0.5000, 0.4995, 0.1586)
150°	(0.5000, 0.4994, 0.1611)	(0.5000, 0.4995, 0.1594)
180°	(0.5000, 0.4997, 0.1599)	(0.5000, 0.4997, 0.1606)

Table S2(aII). Hessian of $\rho(\mathbf{r})$ partitioning scheme measures of the S7-H3 *BCP*s for the 200 GPa *Im-3m*-H_3S crystal graph with variation in the carrier-envelope phase (CEP) angle ϕ corresponding to the 5.0 femtosecond peaks of the **CW (R, [+1])** and **CCW (S, [-1])** pulses, also see **Table S2(aI)**. The total electronic charge density $\rho(\mathbf{r})$, Laplacian $\nabla^2\rho(\mathbf{r})$, metallicity $\xi(\mathbf{r}_b)$, ellipticity ε of the S7-H3 *BCP* are provided, where the S7-H3 *BCP* bond-path length ($BPL_{\%}$ = {(BPL-GBL)/GBL}x100) atomic units are used.

zero E-field

GBL	$\rho(\mathbf{r}_b)$	$\nabla^2\rho(\mathbf{r}_b)$	$\xi(\mathbf{r}_b)$	ε
2.7095	0.1587	-0.1283	-1.2370	0.0000

	CW (R, [+1])					**CCW (S, [-1])**				
ϕ	BPL($BPL_{\%}$)	$\rho(\mathbf{r}_b)$	$\nabla^2\rho(\mathbf{r}_b)$	$\xi(\mathbf{r}_b)$	ε	BPL($BPL_{\%}$)	$\rho(\mathbf{r}_b)$	$\nabla^2\rho(\mathbf{r}_b)$	$\xi(\mathbf{r}_b)$	ε
0°	2.8223(4.16)	0.1585	-0.2114	-0.7499	0.0027	2.8223(4.16)	0.1613	-0.2261	-0.7134	0.0027
30°	2.8223(4.16)	0.1605	-0.2164	-0.7414	0.0030	2.8223(4.16)	0.1592	-0.1357	-1.1737	0.0031
60°	2.8223(4.16)	0.1623	-0.2217	-0.7321	0.0035	2.8223(4.16)	0.1574	-0.2481	-0.6345	0.0036
90°	2.8223(4.16)	0.1635	-0.2268	-0.7210	0.0039	2.8223(4.16)	0.1563	-0.3099	-0.5042	0.0040
120°	2.8223(4.16)	0.1638	-0.2307	-0.7099	0.0040	2.8223(4.16)	0.1561	-0.1001	-1.5588	0.0044
150°	2.8223(4.16)	0.1630	-0.2324	-0.7013	0.0039	2.8223(4.16)	0.1570	-0.1973	-0.7955	0.0041
180°	2.8223(4.16)	0.1614	-0.2286	-0.7058	0.0039	2.8223(4.16)	0.1586	-0.2135	-0.7428	0.0041

Table S2(bI). The fractional coordinates for the H3--H5 *BCP*s of the Hessian of $\rho(\mathbf{r})$ partitioning scheme measures for the 200 GPa *Im-3m*-H_3S crystal graph with variation in the carrier-envelope phase (CEP) angle ϕ corresponding to the 5.0 femtosecond peaks of the **CW (R, [+1])** and **CCW (S, [-1])** pulses, see **Scheme 1** of the main text.

fractional coordinates

zero E-field
(0.5000, 1.0000, 0.2500)

	CW (R, [+1])	**CCW (S, [-1])**
ϕ		
0°	(0.5000, 0.9481, 0.2468)	(0.5000, 0.9504, 0.2467)
30°	(0.5000, 0.9515, 0.2482)	(0.5000, 0.9594, 0.2465)
60°	(0.5000, 0.9697, 0.2508)	(0.5000, 0.9764, 0.2470)
90°	(0.5000, 0.0036, 0.2522)	(0.5000, 0.0035, 0.2476)
120°	(0.5000, 0.0284, 0.2510)	(0.5000, 0.0241, 0.2473)
150°	(0.5000, 0.0392, 0.2491)	(0.5000, 0.0366, 0.2473)
180°	(0.5000, 0.0400, 0.2477)	(0.5000, 0.0417, 0.2479)

Table S2(bII). Hessian of $\rho(\mathbf{r})$ partitioning scheme measures for the H3--H5 *BCP*s at 200 GPa *Im-3m*-H_3S crystal graph with variation in the carrier-envelope phase (CEP) angle ϕ corresponding to the 5.0 femtosecond peaks of the **CW (R, [+1])** and **CCW (S, [-1])** pulses, also see **Table S2(cI)**. The total electronic charge density $\rho(\mathbf{r}_b)$, Laplacian $\nabla^2\rho(\mathbf{r}_b)$, metallicity $\xi(\mathbf{r}_b)$, ellipticity ε of the H3--H5 *BCP* are provided, where the H3--H5 bond-path length ($BPL_{\%}$ = {(BPL-GBL)/GBL}x100) atomic units are used.

zero E-field

GBL	$\rho(\mathbf{r}_b)$	$\nabla^2\rho(\mathbf{r}_b)$	$\xi(\mathbf{r}_b)$	ε
2.8222	0.0553	0.1652	0.3349	0.0006

	CW (R, [+1])					**CCW (S, [-1])**				
	BPL($BPL_{\%}$)	$\rho(\mathbf{r}_b)$	$\nabla^2\rho(\mathbf{r}_b)$	$\xi(\mathbf{r}_b)$	ε	BPL($BPL_{\%}$)	$\rho(\mathbf{r}_b)$	$\nabla^2\rho(\mathbf{r}_b)$	$\xi(\mathbf{r}_b)$	ε
ϕ										
0°	2.9356(4.02)	0.0562	0.1597	0.3521	0.0294	2.9254(3.66)	0.0557	0.1613	0.3456	0.3866
30°	2.9252(3.65)	0.0564	0.1658	0.3403	0.0008	2.8943(2.56)	0.0552	0.1594	0.3464	0.3545
60°	2.8607(1.37)	0.0562	0.1721	0.3265	0.0563	2.8465(0.86)	0.0547	0.1562	0.3503	0.3383
90°	2.8227(0.02)	0.0560	0.1762	0.3178	0.0297	2.8227(0.02)	0.0547	0.1590	0.3437	0.0608
120°	2.8538(1.12)	0.0562	0.1717	0.3274	0.2103	2.8456(0.83)	0.0552	0.1568	0.3523	0.1101
150°	2.8843(2.20)	0.0563	0.1664	0.3385	0.4257	2.8768(1.93)	0.0560	0.1566	0.3576	0.1738
180°	2.8892(2.37)	0.0561	0.1622	0.3458	0.5455	2.8949(2.58)	0.0566	0.1622	0.3488	0.1009

Table S2(cI). The fractional coordinates for the S7---S8 *BCP*s of the Hessian of $\rho(\mathbf{r})$ partitioning scheme measures for the 200 GPa *Im-3m*-H_3S crystal graph with variation in the carrier-envelope phase (CEP) angle ϕ corresponding to the 5.0 femtosecond peaks of the **CW (R, [+1])** and **CCW (S, [-1])** pulses, see **Scheme 1** of the main text.

fractional coordinates

zero E-field
(0.2500, 0.2500, 0.2500)

	CW (R, [+1])	**CCW (S, [-1])**
ϕ		
0°	(0.2297, 0.2845, 0.2314)	(0.2339, 0.2707, 0.2431)
30°	(0.2407, 0.2792, 0.2273)	(0.2277, 0.2616, 0.2558)
60°	(0.2509, 0.2681, 0.2303)	(0.2253, 0.2458, 0.2732)
90°	(0.2568, 0.2584, 0.2366)	(0.2297, 0.2314, 0.2845)
120°	(0.2590, 0.2500, 0.2450)	(0.2406, 0.2273, 0.2793)
150°	(0.2578, 0.2435, 0.2536)	(0.2509, 0.2303, 0.2681)
180°	(0.2543, 0.2386, 0.2616)	(0.2569, 0.2367, 0.2582)

Table S2(cII). Hessian of $\rho(\mathbf{r})$ partitioning scheme measures for the S7---S8 *BCP*s at 200 GPa *Im-3m*-H_3S crystal graph with variation in the carrier-envelope phase (CEP) angle ϕ corresponding to the 5.0 femtosecond peaks of the **CW (R, [+1])** and **CCW (S, [-1])** pulses, also see **Table S2(bI)**. The total electronic charge density $\rho(\mathbf{r}_b)$, Laplacian $\nabla^2\rho(\mathbf{r}_b)$, metallicity $\xi(\mathbf{r}_b)$, ellipticity ε are provided, where the S7---S8 bond-path length ($BPL_{\%}$ = {(BPL-GBL)/GBL}x100) atomic units are used.

zero E-field

GBL	$\rho(\mathbf{r}_b)$	$\nabla^2\rho(\mathbf{r}_b)$	$\xi(\mathbf{r}_b)$	ε
4.8883	0.0557	0.1558	0.3572	0.0006

	CW (R, [+1])					**CCW (S, [-1])**				
ϕ	BPL($BPL_{\%}$)	$\rho(\mathbf{r}_b)$	$\nabla^2\rho(\mathbf{r}_b)$	$\xi(\mathbf{r}_b)$	ε	BPL($BPL_{\%}$)	$\rho(\mathbf{r}_b)$	$\nabla^2\rho(\mathbf{r}_b)$	$\xi(\mathbf{r}_b)$	ε
0°	4.9290(0.83)	0.0516	0.1621	0.3182	0.5813	4.9041(0.32)	0.0529	0.1575	0.3356	0.0784
30°	4.9183(0.61)	0.0529	0.1625	0.3257	0.3427	4.9009(0.26)	0.0515	0.1589	0.3243	0.0485
60°	4.9021(0.28)	0.0547	0.1627	0.3361	0.0806	4.9109(0.46)	0.0511	0.1637	0.3118	0.3589
90°	4.8937(0.11)	0.0565	0.1537	0.3675	0.5089	4.9291(0.83)	0.0516	0.1621	0.3183	0.5691
120°	4.8903(0.04)	0.0578	0.1609	0.3591	0.0781	4.9184(0.62)	0.0529	0.1626	0.3255	0.3417
150°	4.8903(0.04)	0.0583	0.1568	0.3716	0.0732	4.9021(0.28)	0.0547	0.1627	0.3362	0.0771
180°	4.8932(0.10)	0.0578	0.1567	0.3687	0.0435	4.8937(0.11)	0.0565	0.1657	0.3407	0.1682

Table S2(dI). The fractional coordinates for the S7-H3 *BCP*s of the Hessian of $\rho(\mathbf{r})$ partitioning scheme measures for the 200 GPa *Im-3m*-H_3S crystal graph in the absence of an applied **E**-field and also with variation in the carrier-envelope phase (CEP) angle ϕ corresponding to the 15.0 femtosecond peaks of the **CW (R, [+1])** and **CCW (S, [-1])** pulses, see **Scheme 1** of the main text.

	CW (R, [+1])	**CCW (S, [-1])**
ϕ		
0°	(0.5000, 0.5001, 0.1607)	(0.5000, 0.5003, 0.1598)
30°	(0.5000, 0.4997, 0.1608)	(0.5000, 0.4999, 0.1597)
60°	(0.5000, 0.4994, 0.1607)	(0.5000, 0.4996, 0.1597)
90°	(0.5000, 0.4992, 0.1604)	(0.5000, 0.4995, 0.1599)
120°	(0.5000, 0.4991, 0.1602)	(0.5000, 0.4995, 0.1601)
150°	(0.5000, 0.4993, 0.1600)	(0.5000, 0.4996, 0.1605)
180°	(0.5000, 0.4997, 0.1598)	(0.5000, 0.4999, 0.1608)

Table S2(dII). The Hessian of $\rho(\mathbf{r})$ partitioning scheme measures for the 200 GPa *Im-3m*-H_3S crystal graph with variation in the carrier-envelope phase (CEP) angle ϕ corresponding to the 15.0 femtosecond peaks of the **CW (R, [+1]) CCW (S, [-1])** pulses, see **Scheme 1** of the main text. The total electronic charge density $\rho(\mathbf{r}_b)$, Laplacian $\nabla^2\rho(\mathbf{r}_b)$, metallicity $\xi(\mathbf{r}_b)$, ellipticity ε of the S7-H3 *BCP* are provided, where the S7-H3 bond-path length ($BPL_{\%}$ = {(BPL-GBL)/GBL}x100) atomic units are used.

zero E-field

GBL	$\rho(\mathbf{r}_b)$	$\nabla^2\rho(\mathbf{r}_b)$	$\xi(\mathbf{r}_b)$	ε
2.7095	0.1587	-0.1283	-1.2370	0.0000

	CW (R, [+1])					**CCW (S, [-1])**				
ϕ	BPL($BPL_{\%}$)	$\rho(\mathbf{r}_b)$	$\nabla^2\rho(\mathbf{r}_b)$	$\xi(\mathbf{r}_b)$	ε	BPL($BPL_{\%}$)	$\rho(\mathbf{r}_b)$	$\nabla^2\rho(\mathbf{r}_b)$	$\xi(\mathbf{r}_b)$	ε
0°	2.8223(4.16)	0.1584	-0.2097	-0.7554	0.0049	2.8223(4.16)	0.1602	-0.2186	-0.7328	0.0060
30°	2.8223(4.16)	0.1573	-0.2024	-0.7771	0.0045	2.8223(4.16)	0.1612	-0.2254	-0.7150	0.0061
60°	2.8223(4.16)	0.1568	-0.1983	-0.7907	0.0043	2.8223(4.16)	0.1617	-0.2291	-0.7057	0.0063
90°	2.8223(4.16)	0.1569	-0.1977	-0.7935	0.0050	2.8223(4.16)	0.1615	-0.2289	-0.7055	0.0065
120°	2.8223(4.16)	0.1576	-0.2026	-0.7779	0.0056	2.8222(4.16)	0.1607	-0.2250	-0.7144	0.0064
150°	2.8223(4.16)	0.1588	-0.2096	-0.7575	0.0064	2.8222(4.16)	0.1596	-0.2178	-0.7327	0.0061
180°	2.8222(4.16)	0.1600	-0.2134	-0.7497	0.0067	2.8223(4.16)	0.1583	-0.2090	-0.7573	0.0056

Table S2(eI). The fractional coordinates for the H3--H5 *BCP*s of the Hessian of $\rho(\mathbf{r})$ partitioning scheme measures for the 200 GPa *Im-3m*-H_3S crystal graph with variation in the carrier-envelope phase (CEP) angle ϕ corresponding to the 15.0 femtosecond peaks of the **CW (R, [+1])** and **CCW (S, [-1])** pulses, see **Scheme 1** of the main text.

	CW (R, [+1])	**CCW (S, [-1])**
ϕ		
0°	(0.2498, 0.4947, 0.0073)	(0.2498, 0.4946, 0.9928)
30°	(0.2498, 0.4962, 0.0046)	(0.2498, 0.4961, 0.9954)
60°	(0.2498, 0.4987, 0.0005)	(0.2498, 0.4987, 0.9995)
90°	(0.2498, 0.5017, 0.9963)	(0.2497, 0.5017, 0.0036)
120°	(0.2497, 0.5042, 0.9933)	(0.2497, 0.5042, 0.0067)
150°	(0.2497, 0.5055, 0.9921)	(0.2497, 0.5055, 0.0079)
180°	(0.2498, 0.5054, 0.9928)	(0.2498, 0.5053, 0.0073)

Table S2(eII). The Hessian of $\rho(\mathbf{r})$ partitioning scheme measures for the 200 GPa *Im-3m*-H_3S crystal graph with variation in the carrier-envelope phase (CEP) angle ϕ corresponding to the 15.0 femtosecond peaks of the **CW (R, [+1]) CCW (S, [-1])** pulses, see **Scheme 1** of the main text. The total electronic charge density $\rho(\mathbf{r}_b)$, Laplacian $\nabla^2\rho(\mathbf{r}_b)$, metallicity $\xi(\mathbf{r}_b)$, ellipticity ε of the H3--H5 *BCP* are provided, where the H3--H5 bond-path length ($BPL_{\%}$ = {(BPL-GBL)/GBL}x100) atomic units are used, see the caption of **Figure S2(a)** for further details.

zero E-field

GBL	$\rho(\mathbf{r}_b)$	$\nabla^2\rho(\mathbf{r}_b)$	$\xi(\mathbf{r}_b)$	ε
2.8222	0.0553	0.1652	0.3349	0.0006

	CW (R, [+1])					**CCW (S, [-1])**				
ϕ	BPL($BPL_{\%}$)	$\rho(\mathbf{r}_b)$	$\nabla^2\rho(\mathbf{r}_b)$	$\xi(\mathbf{r}_b)$	ε	BPL($BPL_{\%}$)	$\rho(\mathbf{r}_b)$	$\nabla^2\rho(\mathbf{r}_b)$	$\xi(\mathbf{r}_b)$	ε
0°	2.8252(0.11)	0.0560	0.1649	0.3399	0.0879	2.8251(0.10)	0.0560	0.1651	0.3392	0.0803
30°	2.8237(0.05)	0.0560	0.1651	0.3392	0.0879	2.8236(0.05)	0.0560	0.1654	0.3384	0.0815
60°	2.8225(0.01)	0.0560	0.1654	0.3386	0.0826	2.8226(0.01)	0.0560	0.1656	0.3379	0.0848
90°	2.8232(0.04)	0.0560	0.1654	0.3388	0.0823	2.8231(0.03)	0.0560	0.1651	0.3393	0.0830
120°	2.8247(0.09)	0.0561	0.1648	0.3402	0.0810	2.8246(0.09)	0.0561	0.1646	0.3407	0.0855
150°	2.8257(0.12)	0.0561	0.1648	0.3403	0.0800	2.8256(0.12)	0.0561	0.1645	0.3411	0.0875
180°	2.8251(0.10)	0.0561	0.1655	0.3389	0.1022	2.8251(0.10)	0.0561	0.1648	0.3405	0.0871

3. Supplementary Materials S3. Variation of the 200 GPa *Im-3m*-H_3S crystal graph ellipticity ε with time and the carrier-envelope phase (CEP) angle ϕ.

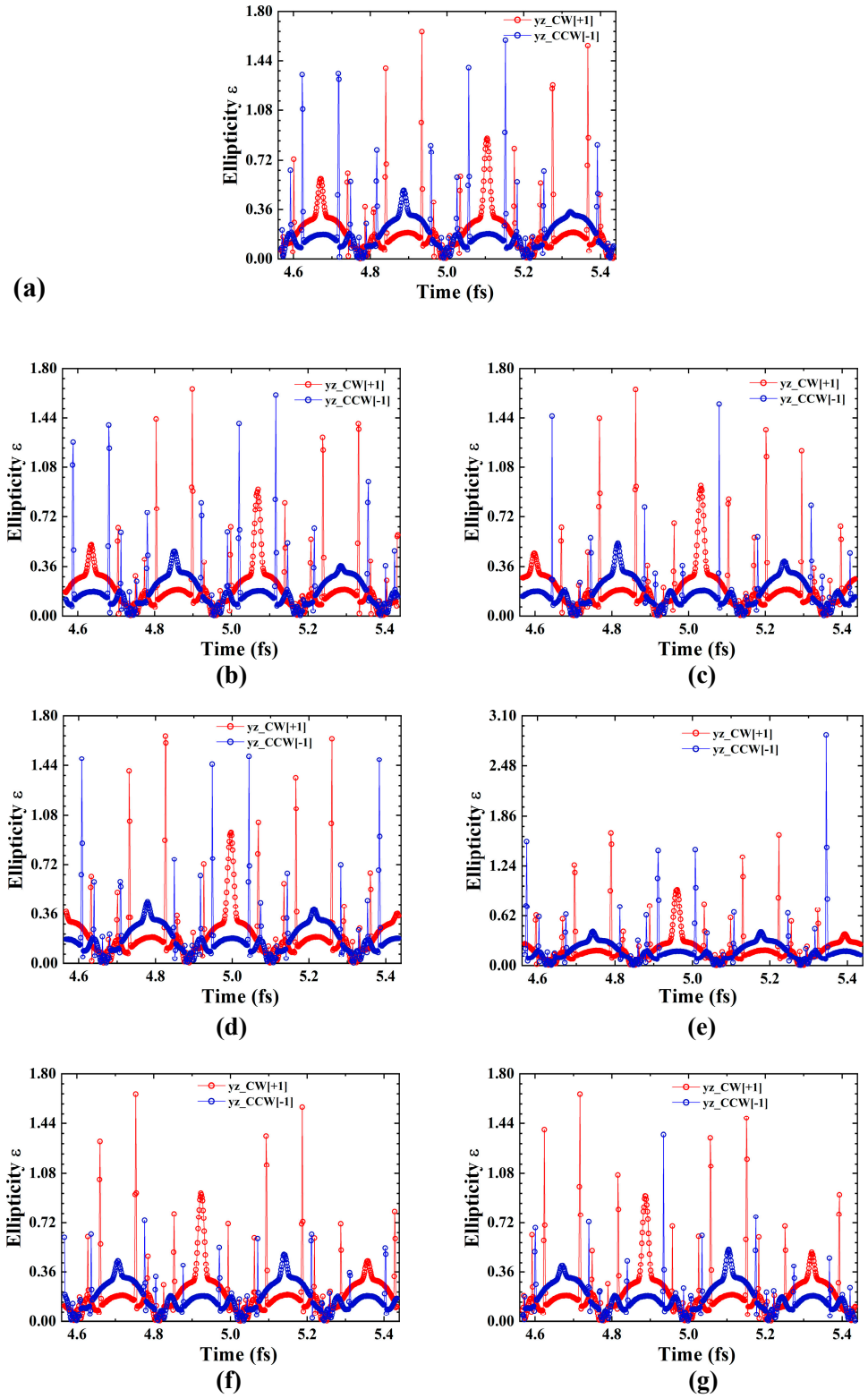


Figure S3(I). The variation of the 200 GPa *Im-3m*-H_3S crystal graph H3--H5 *BCP* ellipticity ε for 5.0 femtosecond peaks of the clockwise (**CW[+1]**), right-handed (**R**) and left-handed, counter-clockwise (**CCW[-1]**), left-handed (**S**) circularly polarized laser pulses for CEP angle ϕ = 0°, 30°, 60°, 90°, 120°, 150°, 180° are presented in sub-figures **(a-g)** respectively. Note the position of the black arrow on the axis indicating the effect of varying the CEP angle ϕ, for further details see **Scheme 1**.

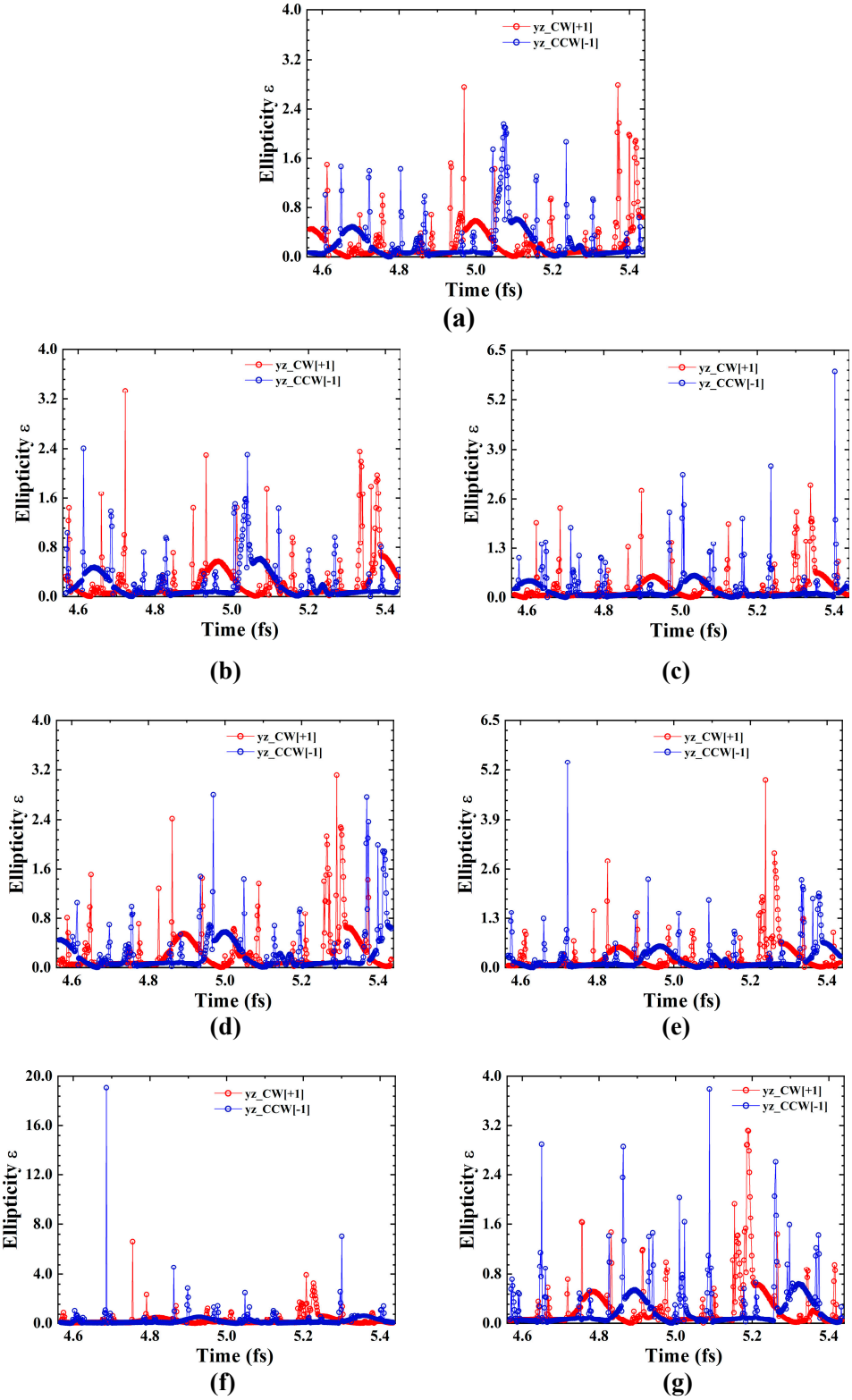


Figure S3(II). The variation of the 200 GPa *Im-3m*-H_3S crystal graph S7---S8 *BCP* ellipticity ε for 5 femtosecond peaks of the clockwise (**CW[+1**]), right-handed (**R**) and left-handed, counter-clockwise (**CCW[-1]**), left-handed (**S**) circularly polarized laser pulses for CEP angle ϕ = 0°, 30°, 60°, 90°, 120°, 150°, 180° are presented in sub-figures **(a-g)** respectively. Note the position of the black arrow on the axis indicating the effect of varying the CEP angle ϕ, for further details see **Scheme 1** of the main text.

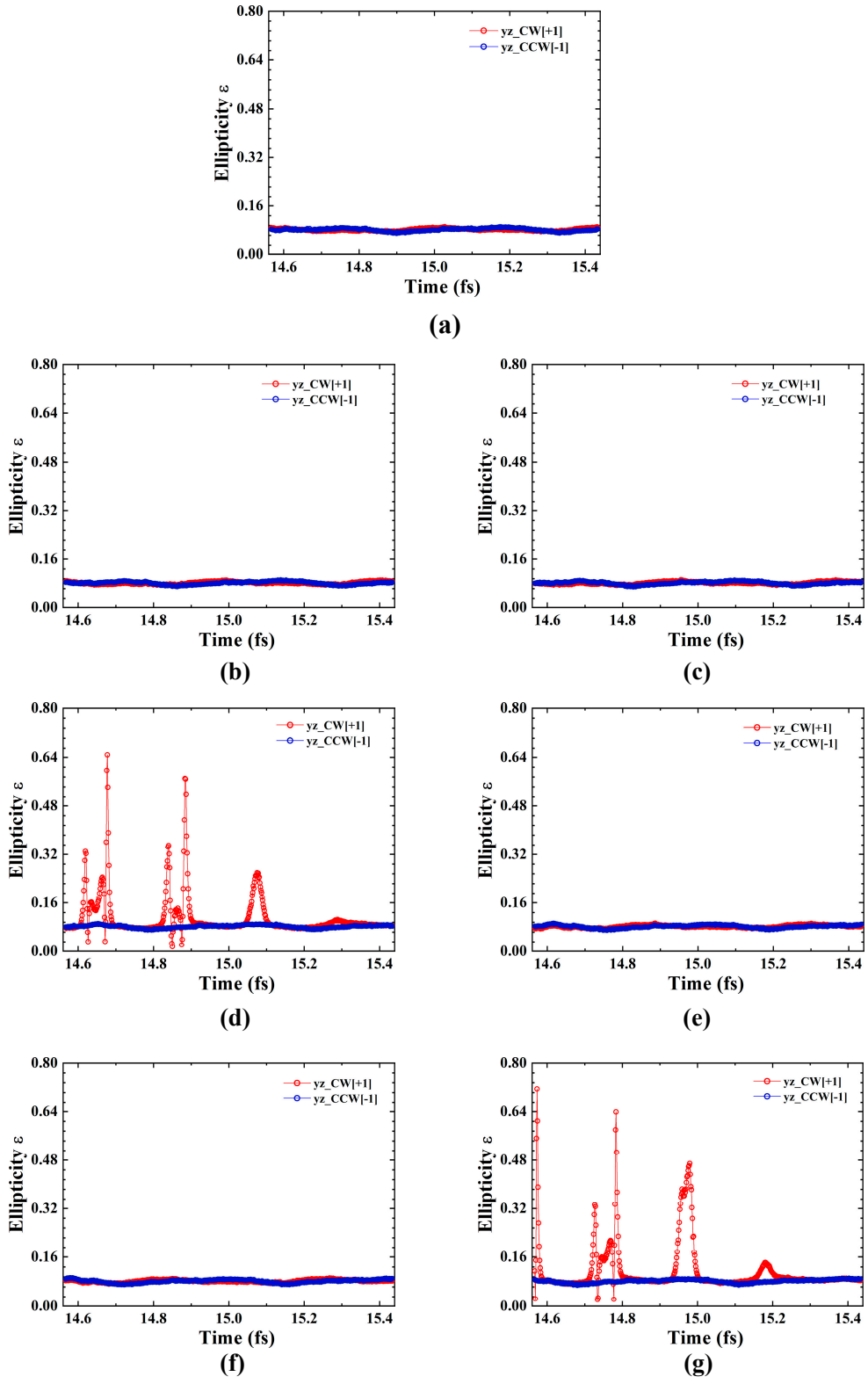


Figure S3(III). The variation of the 200 GPa *Im-3m*-H_3S crystal graph H3--H5 *BCP* ellipticity ε for 15.0 femtosecond peaks of the clockwise (**CW[+1]**), right-handed (**R**) and left-handed, counter-clockwise (**CCW[-1]**), left-handed (**S**) circularly polarized laser pulses for CEP angle ϕ = 0°, 30°, 60°, 90°, 120°, 150°, 180° are presented in sub-figures **(a-g)** respectively. Note the position of the black arrow on the axis indicating the effect of varying the CEP angle ϕ, for further details see **Scheme 1**.

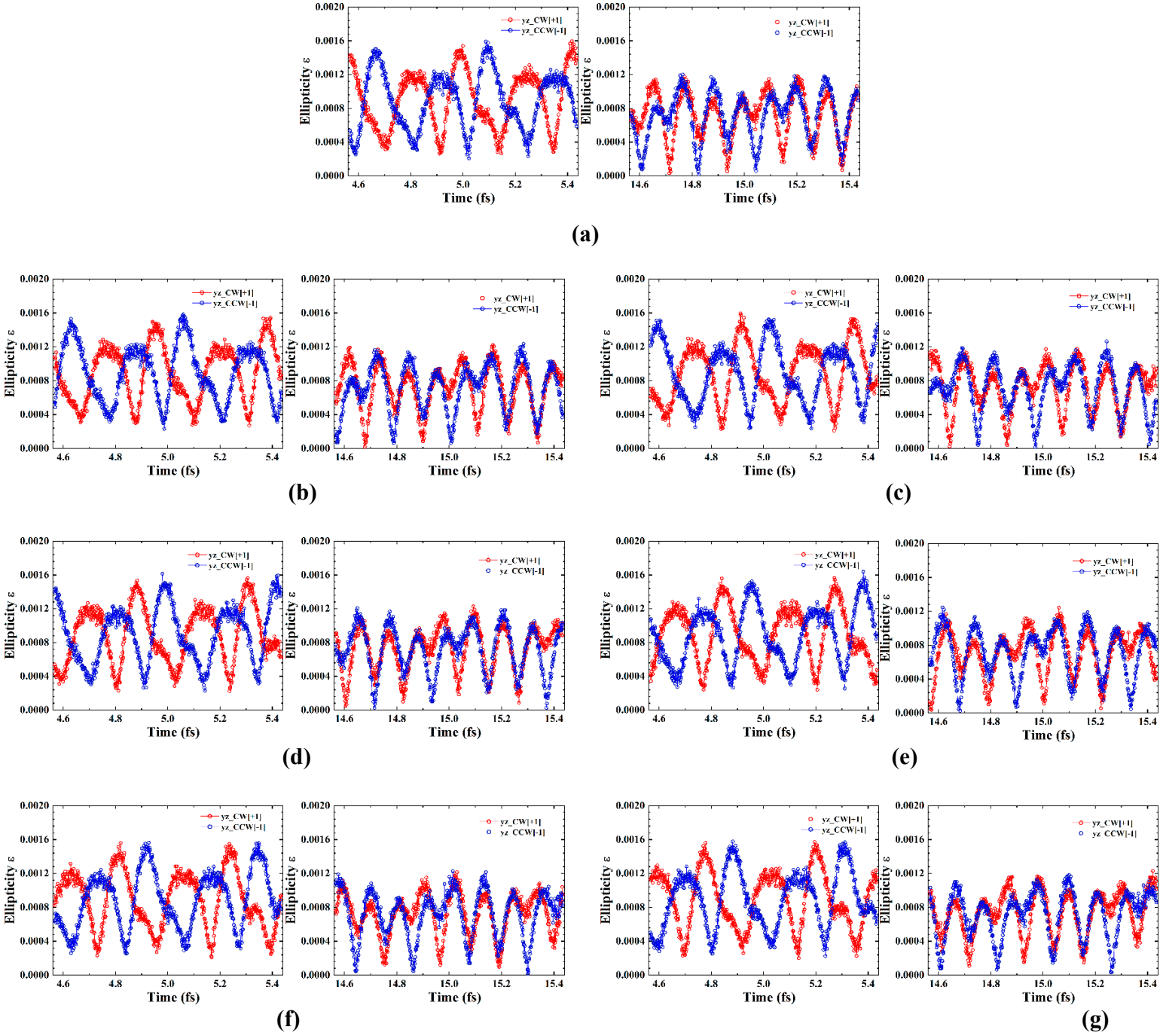


Figure S3(IV). The variation of the *Im-3m*-H_3S crystal graph S7-H1 *BCP* ellipticity ε for 5.0 fs peaks (left panel) and 15.0 fs peaks (right panel) of the clockwise (**R**, CW[+1]), right-handed (red) and counter-clockwise (**S**, CCW[-1]), left-handed (blue) circularly polarized ultra-fast laser pulses in the *yz* plane for the carrier-envelope phase (CEP) angle ϕ = 0°, 30°, 60°, 90°, 120°, 150°, 180° are presented in sub-figures **(a-g)**, respectively.

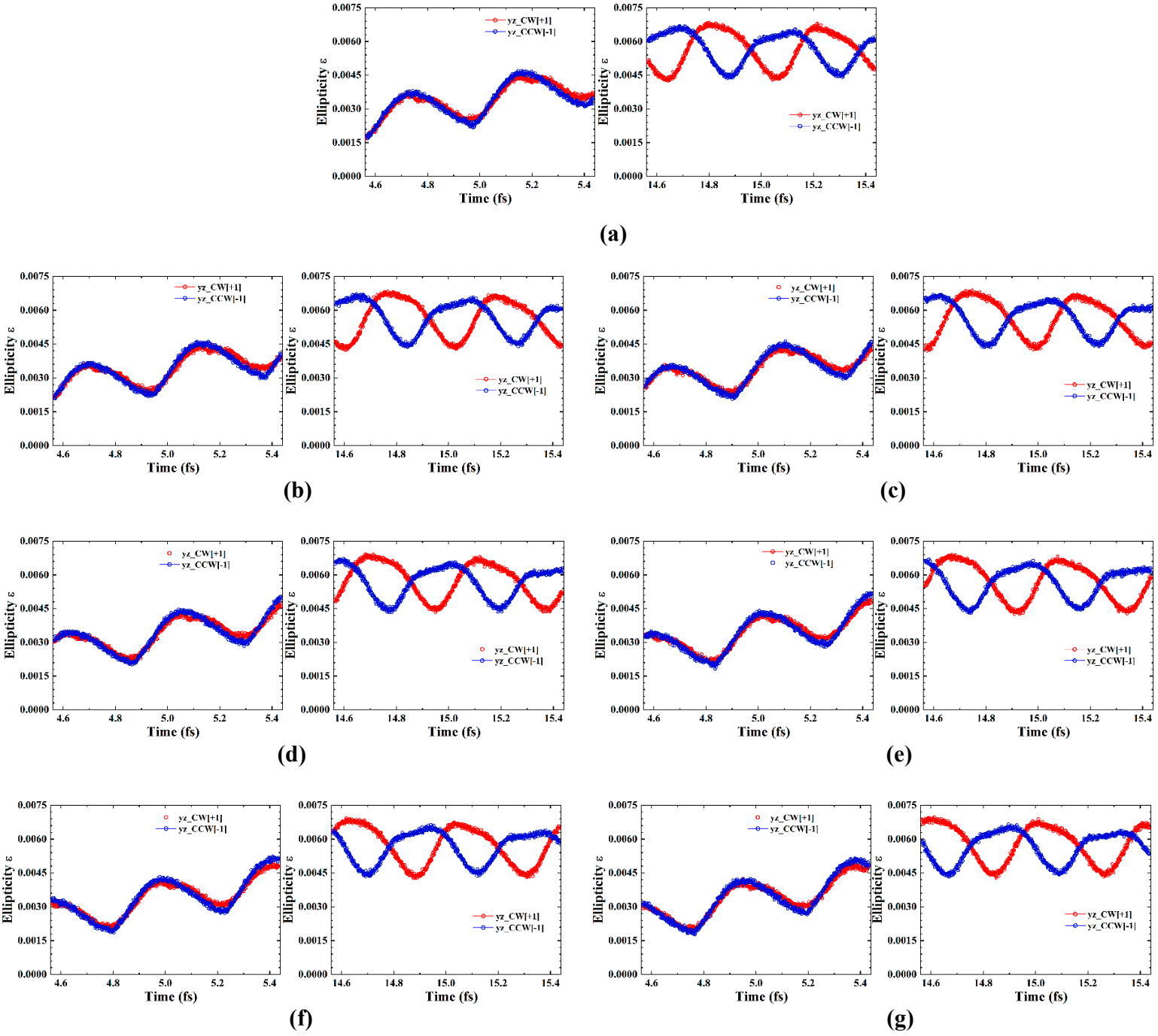


Figure S3(V). The variation of the *Im-3m*-H_3S crystal graph S7-H3 *BCP* ellipticity ε for 5.0 fs peaks (left panel) and 15.0 fs peaks (right panel) of the **R** (red) and **S**) (blue) circularly polarized ultra-fast laser pulses in the *yz* plane for the carrier-envelope phase (CEP) angle $\phi = 0°$ to 180° in increments of 30° are presented in sub-figures **(a-g)** respectively. For further details see the caption of **Figure S3(IV)**.

4. Supplementary Materials S4. Tables and trajectories $\mathsf{T}(s)$ of the 200 GPa *Im-3m*-H_3S crystal graph.

Table S4(a). The maximum Hessian of $\rho(\mathbf{r})$ eigenvector-following trajectory projections $\mathsf{T}_{max}(s)$ = {bond-flexing$_{max}$, chirality$_{max}$, bond-axiality$_{max}$} where F = bond-flexing$_{max}$, C = bond-twist$_{max}$ and A = bond-axiality$_{max}$} of the S7-H1 *BCP* of for values of the carrier-envelope phase angle ϕ = 0°, 30°, 60°, 90°, 120°, 150°, 180° corresponding to the 5.0 femtosecond (fs) peaks of the right-handed **CW (R, [+1])** and left-handed **CCW (S, [-1])]** in the planes of polarization *yz* are provided; all entries have been multiplied by 10^3.

	CW (R, [+1])	**CCW (S, [-1])**
ϕ		
0°	{0.14361792, 0.14382620, 0.01132144}	{0.14382577, 0.14513705, 0.00652208}
30°	{0.14314109, 0.14644309, 0.00554626}	{0.14478203, 0.14287050, 0.01123115}
60°	{0.14304436, 0.14329671, 0.00567880}	{0.14302874, 0.14359628, 0.01076204}
90°	{0.14434132, 0.14298765, 0.00550404}	{0.14345015, 0.14391475, 0.00938055}
120°	{0.14370692, 0.14292723, 0.00546589}	{0.14322136, 0.14352691, 0.00709643}
150°	{0.14359801, 0.14368343, 0.00540661}	{0.14310957, 0.14282864, 0.00542897}
180°	{0.14387781, 0.14224397, 0.00803478}	{0.14430360, 0.14579952, 0.01116124}

Table S4(b). The $\mathsf{T}_{max}(s)$ of the S7-H1 *BCP* for values of the carrier-envelope phase angle ϕ corresponding to the 15.0 fs peaks, see **Table 4(a)** for further details.

	CW (R, [+1])	**CCW (S, [-1])**
ϕ		
0°	{0.16189290, 0.16510606, 0.03766503}	{0.16331054, 0.16550540, 0.03770013}
30°	{0.17008875, 0.17221378, 0.03705974}	{0.16601981, 0.16836675, 0.03798169}
60°	{0.16873888, 0.16557766, 0.03650688}	{0.16517189, 0.16284152, 0.03747466}
90°	{0.16619128, 0.16479468, 0.03834845}	{0.16257862, 0.16596550, 0.03714992}
120°	{0.16513830, 0.16687695, 0.03701266}	{0.16953928, 0.17532036, 0.03672997}
150°	{0.16732713, 0.16382197, 0.03598561}	{0.16812462, 0.16500498, 0.03655100}
180°	{0.16685279, 0.16461051, 0.03625440}	{0.16845828, 0.16555422, 0.03686823}

Table S4(c). The maximum Hessian of $\rho(\mathbf{r})$ eigenvector-following trajectory projections $\mathsf{T}_{max}(s)$ = {bond-flexing$_{max}$,

chirality$_{max}$, bond-axiality$_{max}$} where F = bond-flexing$_{max}$, C = bond-twist$_{max}$ and A = bond-axiality$_{max}$} of the S7-H3 *BCP* of for values of the carrier-envelope phase angle ϕ = 0°, 30°, 60°, 90°, 120°, 150°, 180° corresponding to the 5.0 femtosecond (fs) peaks of the right-handed **CW (R, [+1])** and left-handed **CCW (S, [-1**]**)** in the planes of polarization *yz* are provided; all entries have been multiplied by 10^3.

	CW (R, [+1])	**CCW (S, [-1])**
ϕ		
0°	{0.14624757, 0.00495679, 0.54944810}	{0.14229137, 0.00426725, 0.55486127}
30°	{0.14677713, 0.00307060, 0.55036427}	{0.14333896, 0.00261908, 0.55521248}
60°	{0.14224171, 0.00771291, 0.54972258}	{0.14465235, 0.00508702, 0.55517881}
90°	{0.14190383, 0.00236206, 0.54919713}	{0.14597915, 0.00520566, 0.55408253}
120°	{0.14080769, 0.00200250, 0.55054041}	{0.14691774, 0.00216100, 0.55317457}
150°	{0.14081672, 0.00201695, 0.55128653}	{0.14765547, 0.00530370, 0.55380618}
180°	{0.14184620, 0.00296269, 0.55153486}	{0.14731394, 0.00426728, 0.55428573}

Table S4(d). The T$_{max}$(*s*) of the S7-H3 *BCP* for values of the carrier-envelope phase angle ϕ corresponding to the 15.0 fs peaks, see **Table 6(a)** for further details.

	CW (R, [+1])	**CCW (S, [-1])**
ϕ		
0°	{0.18729833, 0.00216962, 0.12302408}	{0.18764200, 0.00537812, 0.15544693}
30°	{0.18783590, 0.00374074, 0.12586330}	{0.18646426, 0.00299088, 0.15776879}
60°	{0.18150964, 0.00837471, 0.12661534}	{0.18343462, 0.00462663, 0.15869824}
90°	{0.18178930, 0.00689398, 0.13119693}	{0.18419787, 0.00644237, 0.16084643}
120°	{0.18320980, 0.00378008, 0.12256963}	{0.18583325, 0.00349397, 0.16201445}
150°	{0.18425196, 0.00183962, 0.11565064}	{0.18828562, 0.00510637, 0.16733045}
180°	{0.18755773, 0.00169221, 0.11850983}	{0.18852633, 0.00517278, 0.16297866}

Table S4(e). The T$_{max}$(*s*) of the H3--H5 *BCP* for values of the carrier-envelope phase angle ϕ corresponding to the 5.0 fs peaks, see **Table 4(a)** for further details.

	CW (R, [+1])	CCW (S, [-1])
ϕ		
0°	{16.12020147, 2.21605735, 0.78775333}	{0.75139104, 16.33359290, 0.73922393}
30°	{15.94769767, 2.97972577, 1.31850374}	{15.55551151, 4.99395240, 1.13635297}
60°	{15.84596848, 3.18753209, 1.62585252}	{15.05039581, 5.68213732, 1.64728426}
90°	{15.94026079, 2.57507653, 1.74877305}	{15.64968290, 4.43259523, 1.83507948}
120°	{16.06420227, 2.01935465, 1.59750285}	{16.09679901, 2.45064206, 1.56625516}
150°	{16.23363587, 1.14130848, 1.18362333}	{16.09070661, 1.48798199, 1.00660311}
180°	{0.97601436, 16.30798533, 0.66332638}	{15.88697087, 2.91172761, 0.82232744}

Table S4(f). The $\mathsf{T}_{max}(s)$ of the H3--H5 *BCP* for values of the carrier-envelope phase angle ϕ corresponding to the 15.0 fs peaks, see **Table 4(a)** for further details.

	CW (R, [+1])	CCW (S, [-1])
ϕ		
0°	{1.55391427, 2.17166218, 0.02977328}	{1.52942384, 2.18332029, 0.03328097}
30°	{1.53613477, 2.21300196, 0.02881927}	{1.55495991, 2.20444511, 0.02978531}
60°	{1.46005504, 2.29880341, 0.03370183}	{1.48988153, 2.35341984, 0.03338626}
90°	{1.43204456, 2.20569661, 0.04010860}	{1.46282805, 2.21293129, 0.03548896}
120°	{1.36616899, 2.21523008, 0.03967095}	{1.36325275, 2.22823201, 0.03553230}
150°	{1.48347170, 2.17908341, 0.03482473}	{1.51517208, 2.17596101, 0.03256508}
180°	{2.03834823, 1.70570061, 0.03178454}	{1.57376368, 2.16578551, 0.02865957}

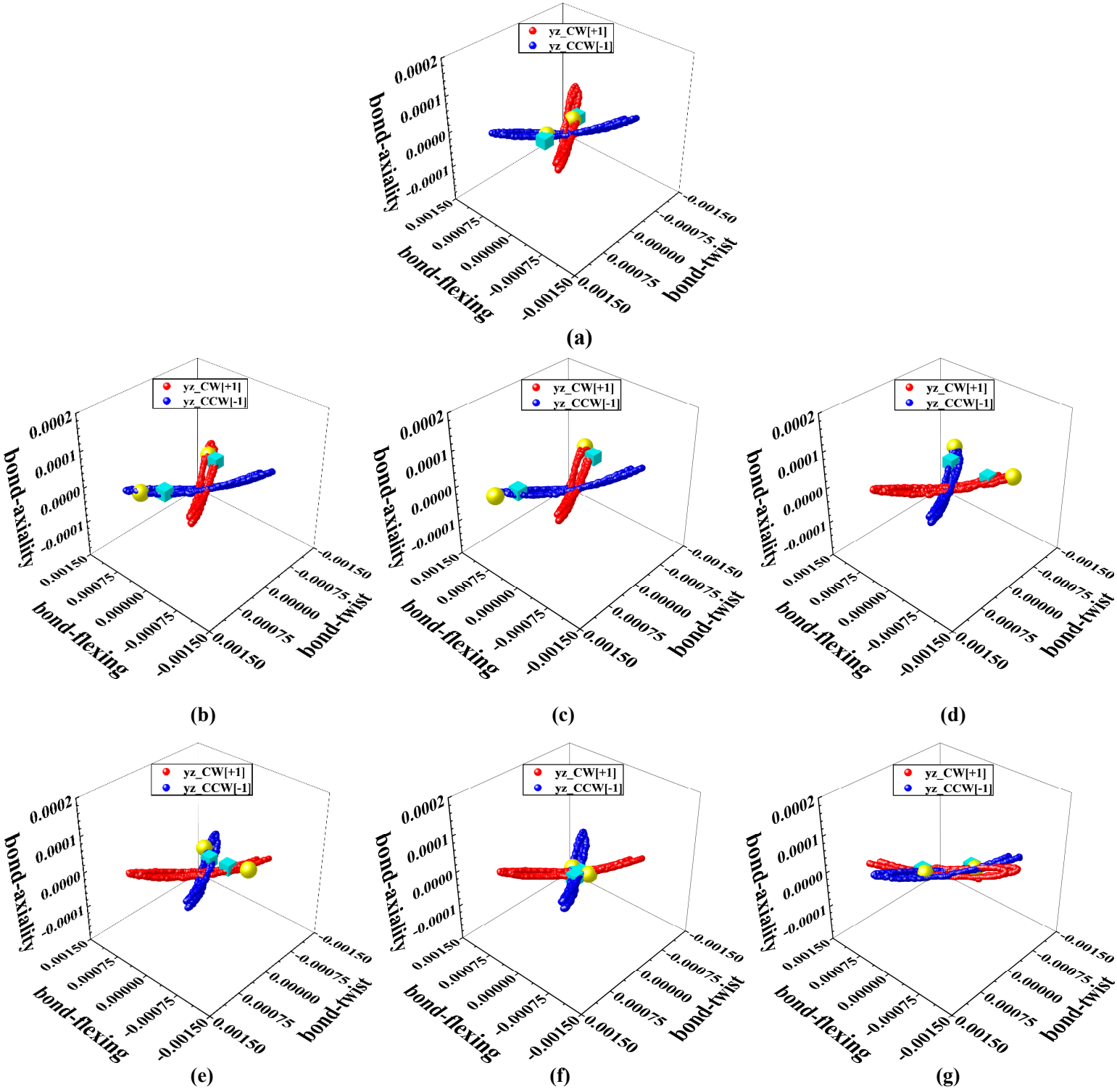


Figure S4. The variation of the *Im-3m*-H_3S crystal graph H3--H5 *BCP* trajectories $\mathsf{T}(s)$ for 15.0 fs peaks of the CW (**R**, red) and the CCW (**S**, blue) circularly polarized laser pulses in the *yz* plane for the CEP angle ϕ = 0°, 30°, 60°, 90°, 120°, 150°, 180° are presented in sub-figures **(a-g)** respectively, see the main text for further details.

5. Supplementary Materials S5. Tables and trajectories $\mathsf{T}(s)$ of the 200 GPa *Im-3m*-H_3S crystal graph S7---S8 *BCP*.

Table S5(a). The $\mathsf{T}_{max}(s)$ of the S7---S8 *BCP* for values of the carrier-envelope phase angle ϕ corresponding to the 5.0 fs peaks, see **Table 4(a)** for further details.

	CW (R, [+1])	**CCW (S, [-1])**
ϕ		
0°	{6.17780949, 9.13341836, 0.89737797}	{6.23536645, 8.16127026, 0.72642464}
30°	{5.49009978, 10.30227140, 0.86568509}	{5.08253506, 8.64029108, 0.74481752}
60°	{5.32253640, 9.24496097, 0.79644496}	{5.56641124, 8.71644035, 0.82131545}
90°	{6.56096065, 8.35452598, 0.74232716}	{6.07210810, 8.65365609, 0.89847584}
120°	{9.12217685, 5.03097662, 0.72805307}	{5.59527785, 8.80793848, 0.86117550}
150°	{9.04156671, 5.27047101, 0.75254343}	{5.47538493, 8.65604119, 0.79503798}
180°	{5.94852794, 8.19836847, 0.73405920}	{6.32979910, 8.38950421, 0.73959188}

Table S5(b). The variation of the S7---S8 *BCP* U-space distortion sets $\{\mathsf{F}, \mathsf{C}, \mathsf{A}\}$ of the crystal graph of the *Im-3m* H_3S unit cell for the variation of the CEP angle ϕ corresponding to 5.0 fs peaks, see the caption of **Table 1(a)** of the main text for further details. Values of the chirality-helicity function $\mathsf{C}_{helicity} = \mathsf{C}|\mathsf{A}|$ are considered insignificant for values of 1.0×10^{-4} or less.

ϕ	$\{\mathsf{F}, \mathsf{C}, \mathsf{A}\}$	$\mathsf{C}_{helicity}$
0°	{-0.05755696, 0.97214810[**S**], 0.17095332}	0.16619
30°	{ 0.40756472, 1.66198032[**S**], 0.12086757}	0.20088
60°	{-0.24387484, 0.52852062[**S**], -0.02487049}	0.01315
90°	{ 0.48885256, -0.29913011[**R**], -0.15614868}	-0.04671
120°	{ 3.52689900, -3.77696185[**R**], -0.13312243}	-0.50280
150°	{ 3.56618178, -3.38557018[**R**], -0.04249455}	-0.14387
180°	{-0.38127116, -0.19113574[**R**], -0.00553268}	-0.00106

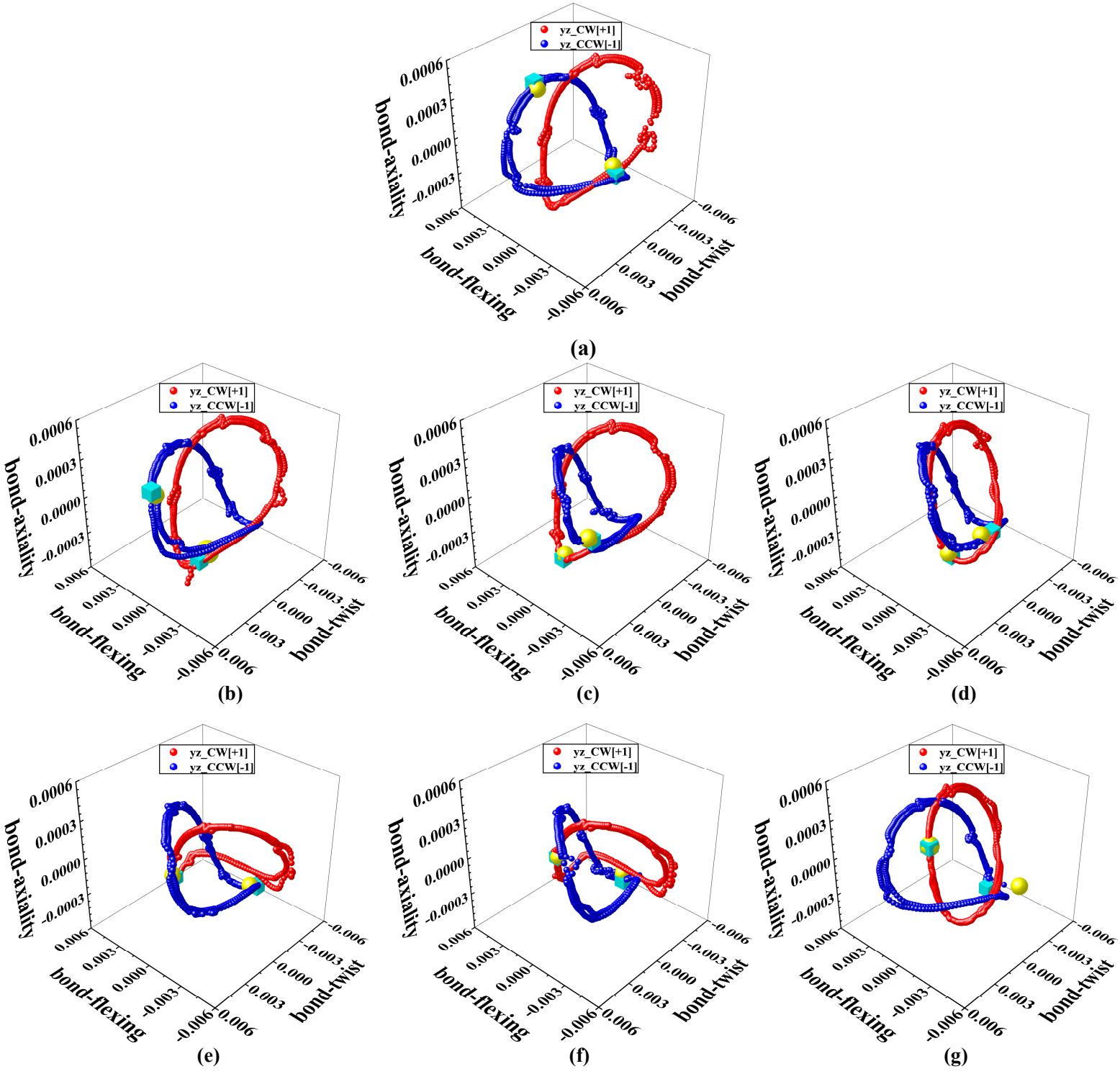


Figure S5. The variation of the *Im-3m*-H_3S crystal graph S7---S8 *BCP* trajectories T(*s*) for 5.0 fs peaks of the clockwise (**CW[+1]**), right-handed (**R**) and left-handed, counter-clockwise (**CCW[-1]**), left-handed (**S**) circularly polarized laser pulses in the *yz* plane for the carrier-envelope phase (CEP) angle ϕ = 0°, 30°, 60°, 90°, 120°, 150°, 180° are presented in sub-figures **(a-g)** respectively. The start and end of each T(*s*) are denoted by balls and cubes respectively.